Liquid Crystals
Publication details, including instructions for authors and subscription information:
http://www.informaworld.com/smpp/title~content=t713926090

Phase diagram of the tetramethylammonium heptadecafluorononanoate (TMAHFN)/D_2O system as determined by ^2H and ^{14}N NMR

J. P. Dombroski[a]; P. J. B. Edwards[a]; K. W. Jolley[a]; N. Boden[b]
[a] Department of Chemistry and Biochemistry, Massey University, Palmerston North, New Zealand [b] Centre for Self Organising Molecular Systems, The University, Leeds, England

To cite this Article Dombroski, J. P. , Edwards, P. J. B. , Jolley, K. W. and Boden, N.(1995) 'Phase diagram of the tetramethylammonium heptadecafluorononanoate (TMAHFN)/D_2O system as determined by ^2H and ^{14}N NMR', Liquid Crystals, 18: 1, 51 — 60
To link to this Article: DOI: 10.1080/02678299508036590
URL: http://dx.doi.org/10.1080/02678299508036590

LIQUID CRYSTALS, 1995, VOL. 18, NO. 1, 51–60

Phase diagram of the tetramethylammonium heptadecafluorononanoate (TMAHFN)/D_2O system as determined by ^2H and ^{14}N NMR

by J. P. DOMBROSKI†, P. J. B. EDWARDS†, K. W. JOLLEY†*
and N. BODEN‡

†Department of Chemistry and Biochemistry, Massey University, Palmerston North, New Zealand.

‡Centre for Self Organising Molecular Systems, The University, Leeds LS2 9JT, England.

(*Received 20 April 1994: accepted 8 June 1994*)

The high resolution phase diagram of the tetramethylammonium heptadecafluorononanoate (TMAHFN)/D_2O system has been mapped out using ^2H and ^{14}N NMR spectroscopy. The ^{14}N quadruple splittings are more than an order of magnitude larger than corresponding ^2H splittings, while the line widths are only two to three times larger. Thus, ^{14}N NMR offers an order of magnitude improvement over ^2H NMR in the resolution of the spectra from coexisting phases. The ^2H spectra of samples in biphasic regions are often complicated by chemical exchange of D_2O molecules between coexisting phases, particularly at low TMAHFN concentrations. Analysis of the ^2H line shapes of a TMAHFN/D_2O sample with a weight fraction of TMAHFN of 0·230 obtained at various times following cooling of the sample into the isotropic/nematic biphasic region shows that the mean diameter for the dispersed nematic droplet grows from about 7 to about 26 μm over a period of 2 h. At a mean droplet size of 7 μm the exchange of TMA^+ ions between the coexisting phases is slow on the NMR time-scale and exchange effects are not observed in ^{14}N spectra. The TMAHFN/D_2O phase diagram exhibits the generic form of those of the CsPFO/water and APFO/D_2O systems, which are the only other systems composed of stable discotic micelles for which high resolution phase diagrams are currently available, but the nematic phase is displaced to smaller TMAHFN concentrations. Specifically, a discotic nematic phase N_D^+, intermediate between an isotropic micellar phase I and a lamellar phase L, exists for weight fractions of TMAHFN between 0·149 ($\phi = 0{\cdot}105$) and 0·420 ($\phi = 0{\cdot}325$) and temperatures between 277·3 and 327·6 K.

1. Introduction

Carboxylic acids with short perfluorocarbon chains are exceptional for their preference to form solutions of discotic micelles which are stable over wide concentration and temperature intervals. This results in generic phase behaviour [1–4] in which the discotic micelles, with increasing concentration, undergo a sequence of disorder–order transitions to form first a nematic phase and, subsequently, a smectic lamellar phase [5, 6]. The nematic phase N_D is characterized by long-range correlations in the orientation of the symmetry axes of the micelles, whilst in the dilute lamellar phase L_D, the micelles are arranged on equidistant planes. At higher concentrations, because of micelle packing constraints and interlayer repulsive forces, more complex lamellar configurations, such as perforated bilayers etc., must ensue, until eventually classical bilayers prevail. Recent neutron diffraction [7] and water diffusion [8] studies on the caesium pentadecafluoro-octanoate (CsPFO)/water and CsPFO/CsCl/water systems propose a lamellar phase of amphiphile layers pierced by irregular water filled holes, with a classical lamellar phase structure being approached at high surfactant/salt concentrations. A discotic lamellar phase cannot, however, be ruled out solely on the basis of scattering experiments and there is good evidence for the existence of the L_D phase, particularly when the isotropic–lamellar transition occurs via a N_D phase [6, 9]. It is not the purpose of the present study to investigate the detailed evolution of the lamellar structure with concentration, and herein we refer to it simply as a lamellar L phase.

The I–N_D–L sequence of transitions is similar [10] to the isotropic–nematic–smectic A sequence observed for thermotropic liquid crystal materials, but with the fundamental difference that restructuring of the micelle on

* Author for correspondence.

0267–8292/95 $10·00

dilution or change in temperature may lead to a situation where the nature of the transition can be drastically different. For this reason there is considerable interest in experimental studies of phase transition in complex micellar liquid crystals, particularly in the CsPFO/D_2O [1, 3, 5–7, 9–19] and CsPFO/H_2O [4, 8, 20–32] systems, for both of which high resolution phase diagrams have been published [1, 3, 4]. Two notable features of these phase diagrams, and of that for ammonium pentadecafluorooctanoate (APFO)/D_2O [2], are an I–N_D^+–L (the plus sign indicates positive diamagnetic susceptibility) triple point (Tp(I, N, L)), above which there is a direct I–L transition, and a tricritical point Tcp on the N_D^+–L transition line.

Changing the counterion and/or the length of the fluorocarbon chain has a significant effect on the phase behaviour. The high-resolution phase diagram for the APFO/D_2O [2] system shows that its phase behaviour is qualitatively similar to that for the CsPFO/water system, with the transition temperatures being about 22 K higher for the Cs^+ salt at corresponding volume fractions. The rubidium salt [27] also exhibits similar phase behaviour to the CsPFO/water system, but its solubility curve is displaced to much higher temperature, and liquid crystal phase behaviour is observed only at high temperatures and concentrations. The sodium and potassium salts are not sufficiently soluble to form liquid crystals, whilst the lithium salt behaves more like a classical soap [33]. Increasing the length of the fluorocarbon chain displaces the I–N_D^+–L sequence of transitions to higher temperatures. For the Cs^+ [34] and NH_4^+ [34, 35] salts, for example, replacing PFO^- by HFN^- results in an increase in the transition temperatures of about 35 K and 45 K, respectively, at corresponding volume fractions. In a recent study on the phase behaviour of micellar liquid crystals formed in aqueous solutions of the Cs^+ salts of tridecafluoroheptanoic, pentadecafluoro-octanoic, heptadecafluorononanoic and nonadecafluorodecanoic acids [36], it was found that the behaviour of all four surfactant systems could be represented on a universal phase diagram in reduced temperature/volume fraction space, i.e. increasing the length of the chain progressively displaces the transitions to higher temperatures, but the I–N_D^+–L transition sequence is preserved and the volume fraction at Tp(I, N, L) and Tcp are about the same.

It is the intrinsic stability of the discotic micelles over wide concentration/temperature ranges that gives rise to the generic phase behaviour outlined above. Simple statistical mechanical models suggest that discotic micelles are intrinsically unstable and should undergo spontaneous growth to form infinite bilayers [37], as is the case for phospholipids, for example. However, McMullen *et al.* [38, 39], using a micelle model consisting of an oblate right-circular cylinder (body) closed by a half-toroidal rim, showed that discotic micelles can be stable, and this requires that the chemical potential of the surfactant in the rim be only slightly greater than that in the body, so that the entropy of mixing suppresses their explosive growth into infinite bilayers. Taylor and Herzfeld [40] have recently considered liquid crystal phases formed in reversibly self-assembling discotic systems (micellar liquid crystals) within the framework of a hard-particle model. Their model allows for polydispersity, which is expected significantly to affect the structure of any translationally ordered phases which occur [41]. The effect of including polydispersity is to favour a translationally ordered lamellar phase consisting of layers of discotic micelles, rather than the characteristic columnar phases exhibited in thermotropic discotic systems. There are many similarities between the topology of their theoretical phase diagram and that for the CsPFO/water [1, 4] and for the APFO/water [2] systems. In particular the theoretical phase diagram reproduces the behaviour along the I–N_D^+ transition with a narrowing of the biphasic isotropic/nematic regime with decreasing aggregate concentration, a displacement of the transition to higher temperatures with increasing aggregate concentration, and an isotropic–nematic–smectic triple point (Tp(I, N, L)) above which there is a direct isotropic–smectic transition. Along the nematic–smectic transition, the agreement is not so good and, in particular, no tricritical point was predicted. This, however, could well be due to limitations in the model for the smectic phase [40, 42].

As part of our study to examine in detail the effects of chain length and counterion on the phase behaviour and self-assembly in perfluoro surfactant/water systems, we have determined the high resolution phase diagram for the tetramethylammonium heptadecafluorononanoate (TMAHFN)/D_2O system. Previous studies have established that this system exhibits a discotic micellar nematic phase, with a positive diamagnetic susceptibility anisotropy [43], which gives rise to monodomain samples in applied magnetic fields, but the available phase diagrams [34, 35, 43] are primitive and they are neither of a standard to allow a detailed comparison between this and other well defined experimental systems [1, 2, 4] nor of sufficient quality to be useful in comparing experimental with theoretical phase behaviour [40] in self-assembling molecular systems.

The method used to map the phase diagram was mainly NMR, both ^2H NMR of heavy water [1–3] and ^{14}N NMR of the counterion. The TMAHFN/D_2O system presents certain experimental difficulties not experienced for the CsPFO/water [1, 3, 4] and APFO/D_2O [2] systems, the phase diagrams for which were determined using mainly either ^2H or ^{133}Cs NMR. TMAHFN/D_2O samples are extremely viscous, have long magnetic relaxation times, and in biphasic regions complications in ^2H spectra as a

consequence of chemical exchange of D_2O molecules between the phases cause considerable problems in the determination of transition temperatures, particularly for samples with low surfactant concentrations. In addition, the TMAHFN/D_2O system exhibits a phenomenon not present in either the CsPFO/water or APFO/D_2O systems, in that surface orientation of the lamellar director occurs on passing through biphasic N_D^+/L or I/L regions. The chemical exchange problem can be overcome by using ^{14}N NMR to determine phase transition temperatures. The magnitude of the ^{14}N quadruple splittings is more than an order of magnitude greater than the ^2H splittings, and ensure that no chemical exchange effects are observed in ^{14}N spectra. The advantages gained from the larger ^{14}N quadrupole splittings outweigh the disadvantage of the lower sensitivity of the ^{14}N nucleus. To our knowledge, this is the first time that ^{14}N NMR has been used for the precise location and characterisation of phase transition temperatures.

2. Experimental methods

2.1. *NMR spectroscopy*

^2H and ^{14}N NMR spectra were measured with a JEOL GX270 spectrometer operating at 41·34 and 19·38 MHz, respectively. The ^2H free induction decays were sampled using 2 K data points over a frequency range of 1 kHz, whilst for the ^{14}N measurements, 8 K data points over a 10 kHz frequency range were usually employed, giving resolutions after Fourier transformation of, respectively, 1 Hz and 2·5 Hz per data point. The sample temperatures were controlled using a double-pass water-flow control system designed to minimize temperature gradients and with an accuracy, precision, and settability of ± 0·005 K [44].

2.2. *Density measurements*

The density of a 0·099547 mol kg^{-1} solution of TMAHFN in H_2O at 25°C was determined using an Anton-Paar vibrating-tube digital-density meter (Model DMA 60/602). The solution density was measured relative to that of pure water (triply distilled under a nitrogen atmosphere) and the apparent molar volume (V_ϕ) of the salt was calculated from the relationship

$$V_\phi = \frac{1000}{mdd_0}(d_0 - d) + \frac{M}{d}$$

where m is the molality of the solution, M is the relative molar mass of the surfactant, d is the density of the solution (1·017511 g cm^{-3}) and d_0 is the density of the solvent (0·997047 g cm^{-3} at 25°C [45]). The calculated V_ϕ of 325·3 cm^3 mol^{-1} corresponds to a TMAHFN density of 1·651 g cm^{-3}. The solution concentration was chosen to be well above the cmc, but at a concentration where the viscosity allowed for easy loading into the cell. The cmc at 25°C was $4{\cdot}5 \times 10^{-3}$ mol kg^{-1} (cf. $2{\cdot}6 \times 10^{-3}$ mol kg^{-1} for heavy water solutions of CsPFO [4] and APFO [46]) as determined from electrical conductivity measurements.

2.3. *Materials and sample preparation*

TMAHFN was prepared by neutralizing an aqueous solution of heptadecafluorononanoic acid (Riedal de Haën) with 10 per cent tetramethylammonium hydroxide (Merck Ltd.). The neutralized solution was freeze dried, and the salt was recrystallized twice from a 50 per cent v/v solution of *n*-hexane and *n*-butanol. The recrystallized salt was placed in a vacuum desiccator for several days to remove all traces of the recrystallizing solvent.

NMR measurements were made on ten samples in a TMAHFN weight fraction w range from 0·15 to 0·49. The samples were prepared by weighing TMAHFN and D_2O directly into 5 mm o.d. NMR tubes which were then flame sealed. Samples were stored at room temperature and gave consistent NMR measurements over the period of the study (6 months), providing care was taken to ensure a homogeneous sample. Mixing was accomplished by heating the sample into the isotropic phase and successively inverting the sample tube. Since the samples were highly viscous this process is time consuming, but it is absolutely essential for the determination of precise, accurate, and reproducible phase transition temperatures [15].

3. Results and discussion

A partial phase diagram for the TMAHN/D_2O system is given in figure 1 and the coefficients for the polynomials from which it is constructed are given in the table. The transition temperatures calculated from the polynomials agree with the experimental values to within ± 0·2 K. The phase diagram shows an N_D^+ phase intermediate between an isotropic micellar solution phase I and a lamellar L phase. The N_D^+ phase is seen to be stable between w of 0·149 (volume fraction $\phi = 0{\cdot}105$) and 0·420 ($\phi = 0{\cdot}325$) and temperatures of 277·3 and 327·6 K. The lamellar–nematic tricritical point Tcp is at $w = 0{\cdot}20(2)$ ($\phi = 0{\cdot}14(2)$), with a corresponding temperature of 286(5) K. The other singular points to note are the critical end point Cep ($T = 277{\cdot}5(2)$ K, $w = 0{\cdot}164$ ($\phi = 0{\cdot}116$)) where the line of second order L–N_D^+ transitions intersects the solubility curve T_c, the I/N_D^+/L triple point Tp(I, N, L) ($T = 327{\cdot}60(5)$ K, $w_I = 0{\cdot}416(1)$ ($\phi_I = 0{\cdot}322$), $w_N = 0{\cdot}420(1)$ ($\phi_N = 0{\cdot}325$), and $w_L = 0{\cdot}427(1)$ ($\phi_L = 0{\cdot}332$)), and the I/N_D^+/K triple point Tp(I, N, K) ($T = 277{\cdot}3(2)$ K, $w_I = 0{\cdot}148(1)$ ($\phi_I = 0{\cdot}104$), $w_N = 0{\cdot}149(1)$ ($\phi_N = 0{\cdot}105$), $w_K = 1{\cdot}0$). Before comparing this phase diagram with those obtained for other perfluorinated systems, aspects of

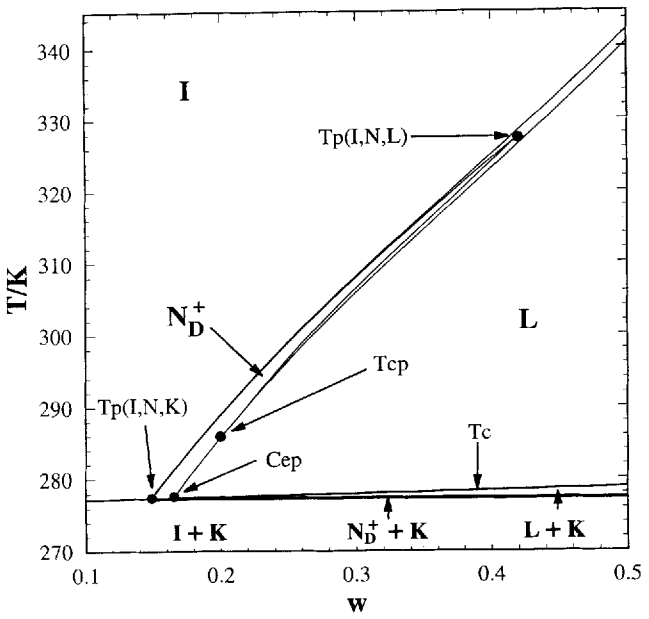

Figure 1. Partial diagram for the TMAHFN/D_2O system. Nomenclature: I, isotropic micellar solution phase; N_D^+, nematic phase with discotic micelles and positive diamagnetic susceptibility; L, lamellar phase; K, crystal; *T*p(I, N, L), the isotropic micellar solution–nematic–lamellar triple point; *T*p(I, N, K), the isotropic micellar solution–nematic–crystal triple point; *C*ep, the critical end point; *T*cp, the lamellar–nematic tricritical point; *T*c, the solubility curve.

the experiments used to establish the transition lines and the fixed points will be discussed.

3.1. *Solubility curve T_c*

Five samples were prepared in the concentration range $w = 0{\cdot}1$ to $0{\cdot}5$. On cooling these samples below T_c, crystallization of the supercooled samples did not occur. In order to achieve crystallization, it was necessary to cool below the freezing point of D_2O. This was done by dipping the samples, which were contained within sealed glass phials, into liquid nitrogen. Once crystallization was achieved, the samples were placed in a hole drilled in a copper block maintained at a temperature of 275 K by water circulating from a Colora cryostat. The temperature was then gradually raised in steps of 0·2 K, waiting for 15 min at each temperature, until the crystals were observed to redissolve completely. This temperature was taken to define a point on the solubility curve. The method worked well, since, over the sample concentration range, the crystals do not undergo macroscopic separation from solution on crystallization and homogeneous remixing takes place on reheating.

3.2. *Liquid crystal transition lines*

These were precisely located by either ^2H or ^{14}N NMR. The NMR spectrum for $I = 1$ nuclei in a macroscopically aligned uniaxial nematic or lamellar mesophase is a doublet with separation $\Delta\tilde{\nu}$, referred to as the partially averaged quadrupole splitting, given by [1]

$$\Delta\tilde{\nu}(\phi) = \tfrac{3}{2}|\tilde{q}_{zz}|_s S P_2(\cos\phi), \qquad (1)$$

where ϕ is the angle between the director **n** and the magnetic field **B**, S is the second-rank orientational order parameter representing the ensemble average of the orientational fluctuations of the micellar axes with respect to **n**, and $|\tilde{q}_{zz}|_s$ is the partially averaged component of the nuclear quadrupole–electric field gradient interaction tensor measured parallel to **n** in a perfectly ordered mesophase. In the vertical bore magnet used in this study, the direction of **B** is along the long axis of the cylindrical sample tube and for macroscopically aligned samples ($\phi = 0°$) $P_2(\cos\phi) = 1$.

For ^2H nuclei in heavy water $|\tilde{q}_{zz}|_s$ is given by [1]

$$|\tilde{q}_{zz}|_s = \langle P_2(\cos\alpha)\rangle_s \chi_D (x_A/x_W) n_b S_{OD}, \qquad (2)$$

where χ_D is the quadrupole coupling constant for a water molecule, x_A and x_W are, respectively, the mole fractions of amphiphile and water, n_b is the number of water molecules bound to each surfactant molecule, and S_{OD} is an 'order parameter' representing the averaging due to the local reorientational motion of these water molecules. The quantity $\langle P_2(\cos\alpha)\rangle_s = \langle \frac{3}{2}\cos^2\alpha - \frac{1}{2}\rangle_s$ where α is the angle between the normal to the surface and the symmetry axis of the micelle, and the angular brackets denote an average over the surface, accounts for the diffusive motion of the molecule over the surface of a discotic micelle. This quantity can be calculated from the axial ratio *a/b* of the micelles [1].

For ^{14}N nuclei $|\tilde{q}_{zz}|_s$ is given by [3, 4]

$$|\tilde{q}_{zz}|_s = \langle P_2(\cos\alpha)\rangle_s \chi_N \beta, \qquad (3)$$

where χ_N is the quadrupole coupling constant for the TMA^+ ion, and β is the fraction of ions which are bound. The observation of a finite quadruple splitting implies that for the fraction of ions β which are bound the methyl groups must be distorted from spherical symmetry.

^{14}N spectra in various phases of a $w = 0{\cdot}372$ sample are shown in figure 2. In the isotropic micellar solution phase I (see figure 2 (*a*)) the spectrum is a singlet, consistent with $S = 0$ (equation (1)). On cooling below T_{IN}, the upper boundary to the I–N_D^+ transition, a symmetrical doublet from the TMA^+ ions in the nematic phase is superimposed on the isotropic singlet (see figure 2 (*b*)). With further cooling, the doublet intensity increases as the singlet intensity decreases until, below T_{NI}, the lower boundary to the I–N_D^+ transition, only the nematic doublet is observed (see figure 2 (*c*)), the splitting of which increases with

Coefficients of the polynomials ($T/K = aw^3 + bw^2 + cw + d$) used to construct the phase diagram for the TMAHFN/D_2O system shown in figure 1. The transition temperatures calculated from these polynomials agree to within ± 0·2 K with the experimental values.

Transition	w range	a	b	c	d
T_{IL}/T_{IN}	0·14–0·50	469·9756	− 532·7108	367·5143	233·0826
T_{NI}	0·14–0·42	371·6179	− 464·2751	351·8064	234·1196
T_{NL}	0·20–0·42	923·6883	− 1002·417	535·0205	211·1939
T_{LN}/T_{LI}	0·16–0·50	552·5171	− 637·621	413·9055	224·0954
Tc	0·10–0·50	0	0	4·1	276·7

decreasing temperature (see figure 2 (*d*)). On cooling below T_{NL}, the upper boundary to the N_D^+–L transition, a second doublet appears symmetrically disposed with respect to the nematic doublet (see figure 2 (*e*)). The discontinuity in the quadrupole splitting is characteristic of a first order nematic–lamellar transition. For a second order transition, there is no mixed phase region and no discontinuity in quadrupole splitting at the transition [1]. On cooling below the lower boundary to the transition T_{LN}, the nematic doublet vanishes and only the lamellar doublet is observed (see figure 2 (*f*)). In figure 2 (*e*), 90° singularities appear in the L phase spectrum, consistent with surface ordering of the L phase director such that it is perpendicular to the direction of **B** (i.e. $P_2(\cos\phi) = 1/2$ in equation (1)). These singularities were only observed in samples on cooling through either biphasic N_D^+/L or I/L regions and were also present in corresponding ^2H spectra (see figure 5). The $\phi = 90°$ peaks correspond to the so-called 'ridge' observed in a SANS study [43] of a macroscopically aligned $w = 0·3$ sample in which the neutron beam was perpendicular to the aligning magnetic field. In a sample in which the neutron beam and aligning field were parallel, no 'ridge' was observed.

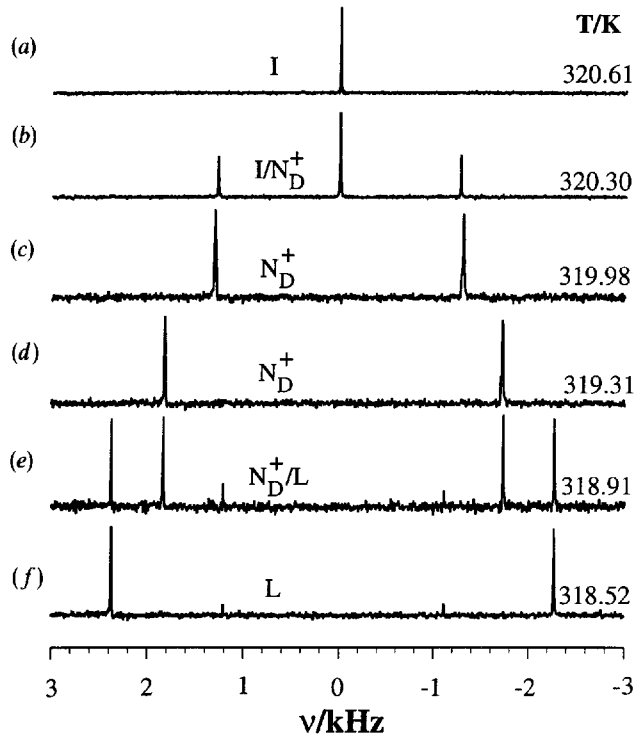

Figure 2. ^{14}N NMR spectra of a TMAHFN/D_2O ($w = 0·372$) sample in (*a*) the isotropic phase, I, (*b*) the isotropic/nematic, I/N_D^+, biphasic region, (*c*) and (*d*) the nematic, N_D^+, phase, (*e*) the nematic/lamellar, N_D^+/L, biphasic region, and (*f*) the lamellar, L, phase. The small peaks in the centre of (*e*) and (*f*) are caused by surface orientation of the L director by the walls of the cylindrical NMR tube such that it is perpendicular to B, i.e. $\phi = 90°$. Thus, the quadrupole splitting of these peaks is given by $\Delta\tilde{\nu}(90°) = 3|q_{zz}|_S S/4$ in contrast to $\Delta\tilde{\nu}(0°) = 3|q_{zz}|_S S/2$ for the large L phase peaks. 500 repetitions we used to obtain the spectra shown in this figure, but quadrupole splittings could readily be extracted from spectra collected after 32 repetitions (total spectrum accumulation time of 32 s).

Magnetic relaxation times [12] were much longer in the TMAHFN/D_2O system compared with those experienced in both the CsPFO and APFO/D_2O systems and, on cooling into the ordered nematic phase, an equilibration time was needed before the quadrupole splittings became constant, as a macroscopically ordered sample was produced. At low surfactant concentrations (low temperatures; high viscosity's; high rotational viscosity's), this time was as long as 1 hour, whilst for the high concentration samples it was only a matter of minutes. Once macroscopic ordering had been achieved, thermal and orientational equilibrium times of the order of 10 min were needed between temperature changes before the quadrupole splittings again became constant.

The linewidths of the ^{14}N peaks in figure 2 are ≈ 9 Hz; these are much smaller than those experienced in the APFO/D_2O system, as are the quadrupole splittings. For a $w = 0·45$ APFO/D_2O sample at T_{LN} (296·32 K), the ^{14}N quadrupole splitting is 34·7 kHz and the linewidth is 0·4 kHz [2]. The differences are due to a greater electric field gradient at the nucleus in the case of the NH_4^+ ion (greater χ_N) associated with a larger distortion from spherical symmetry of the bound NH_4^+ ion compared with that induced in a bound TMA^+ ion.

^{14}N NMR was usually found to be the best method for the determination of the phase transition temperatures.

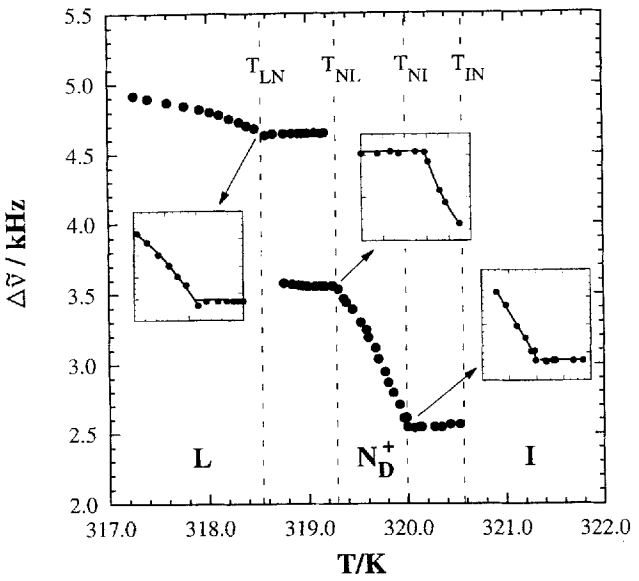

Figure 3. Temperature dependence of the partially averaged ^{14}N quadrupole splittings $\Delta\tilde{\nu}$ for the TMAHFN/D_2O ($w = 0{\cdot}372$) sample the spectra for which are shown in figure 2. The phase transition temperatures T_{NI}, T_{NL}, and T_{LN} are readily identified from the discontinuities in the $\Delta\tilde{\nu}$ versus temperature curves.

The larger quadrupole splittings ensured that complications due to chemical exchange of nuclei between phases in biphasic regions [1, 3] are not experienced and the T_{NI}, T_{NL}, and T_{LN} transition temperatures are readily obtained from the temperature dependence of the ^{14}N quadrupole splittings, as shown in figure 3 for the $w = 0{\cdot}372$ sample (see figure 2 for the appearance of the spectra for this sample). For samples with a concentration less that that of T_{cp} ($w = 0{\cdot}2$), there is no discontinuity in the quadrupole splittings at the N_D^+–L transition, but there is a discontinuity in the temperature dependence which identifies T_{LN} [1, 2, 4].

The appearance of the $w = 0{\cdot}372$ ^2H spectra are similar to those shown in figure 2, but the ^2H quadrupole splittings are more than an order of magnitude smaller than the ^{14}N splittings. At T_{NI}, T_{NL}, and T_{LN}, the magnitudes of the ^{14}N quadrupole splittings are, respectively, 2·54, 3·56 and 4·64 kHz, whilst the corresponding ^2H values are 0·15, 0·21 and 0·27 kHz. This is a consequence of the differences in the two quantities $\chi_D n_b S_{OD} x_A / x_W$ and $\chi_N \beta$ which appear in equations (2) and (3), respectively. Because of the smaller ^2H quadrupole splittings, chemical exchange effects are often observed in biphasic regions and make the detection of the phase transition temperatures difficult. This is particularly so for the low concentration samples, since the ^2H quadrupole splittings decrease with decreasing w as a result of the concomitant decrease in x_A/x_W (equation (2)). Figure 4 shows the appearance of the spectra for a $w = 0{\cdot}23$ sample at various times following cooling from the I (see figure 4 (*a*)) into the biphasic I/N_D^+ region (figure 4 (*b*)–(*e*)). On cooling below T_{IN}, the nematic phase nucleates as a dispersion of small droplets in a matrix of the isotropic phase [1]. D_2O molecules exchange rapidly between the two phases and in the fast exchange limit, a doublet (see figure 4 (*b*)) is observed with a splitting corresponding to the weighted mean of those for the nematic and isotropic phases, i.e. $\Delta\tilde{\nu} = p_N \Delta\tilde{\nu}_N$, where p_N is the population of D_2O molecules in the nematic phase and $p_I + p_N = 1$.

The spectra were fitted using Abragham's equations [47, 48] for two-site chemical exchange. The input parameters were $\Delta\tilde{\nu}_N$ (70 Hz) and p_I (0·43), which were obtained from the slow exchange spectrum (see figure 4 (*e*)), and the spin–spin relaxation time T_2^* (0·2 s), which was obtained from the linewidth at half maximum amplitude of the I phase signal (see figure 4 (*a*)). The mean time interval τ ($\tau = p_N \tau_I = p_I \tau_N$) between successive transfers of molecule between phases was adjusted to give the best agreement between experimental and theoretical spectra, as defined by a minimum in the least squares deviation between experimental and calculated points. The best fit spectra, together with their corresponding τ

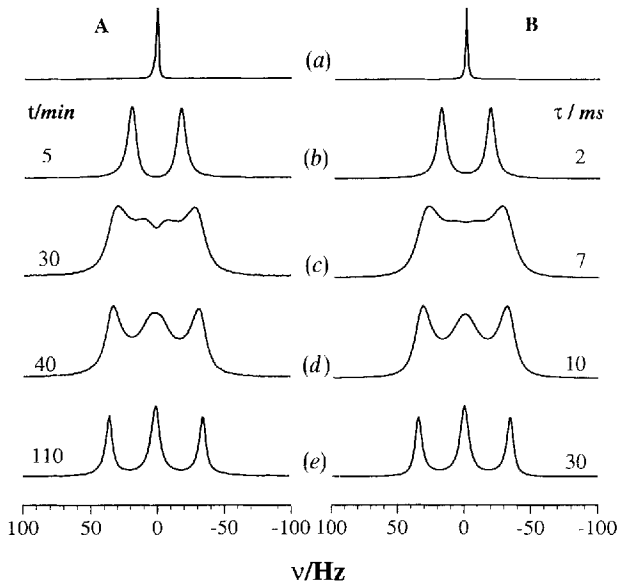

Figure 4. Observed (*A*) and calculated (*B*) ^2H NMR spectra of D_2O for a sample of TMAHFN/D_2O ($w = 0{\cdot}230$) at various times t following cooling from the I phase (*a*) into the I/N_D^+ biphasic region (*b*) to (*e*). The spectrum gradually changes from one in which there is fast exchange of D_2O molecules between the two phases (*b*), through intermediate exchange regions (*c*) and (*d*), into the slow exchange spectrum of (*e*). The transition from fast to slow exchange spectra is associated with growth in the nematic droplets, with a corresponding growth in the mean time interval τ between successive transfers of molecules between phases (see text).

values are shown alongside the experimental spectra in figure 4. The agreement between the spectra is good considering that no account has been taken of polydisperity in droplet sizes in calculating the theoretical lineshapes. A rough idea of the mean droplet size can be obtained by calculating the root mean square distance travelled by a D_2O molecule during the time τ. In 2 ms (see figure 4 (*b*)), a D_2O molecule (diffusion coefficient $\approx 10^{-9}\,m^2\,s^{-1}$) would diffuse a root mean square distance of $(6D\tau)^{1/2}$ or 3·5 μm. Thus the average droplet diameter at this instant will be about 7 μm, and over the following 105 min it grows to about 26 μm. The ^{14}N $\Delta\tilde{\nu}_N$ for the $w = 0{\cdot}230$ sample is 2050 Hz and slow exchange of TMA^+ ion between phases requires $1/\tau < 2\pi\Delta\nu_N$, i.e. $\tau > 8 \times 10^{-5}$ s, which corresponds to a droplet diameter of only about 1·4 μm. Thus no exchange effects are observed in the ^{14}N spectra.

For samples with $w < 0{\cdot}230$, the effects of chemical exchange in ^2H spectra become more pronounced. For a $w = 0{\cdot}184$ sample, $\Delta\tilde{\nu}_N$ is only 50 Hz and slow exchange was achieved after about 3 h, whilst for the lowest concentration sample studied ($w = 0{\cdot}153$), separate I and N_D^+ signals could not be detected at all in the ^2H spectrum of the mixed phase region. In this latter sample, the ^{14}N $\Delta\tilde{\nu}_N$ is 1·4 kHz and the I/N_D^+ spectra were slow exchange ones.

^2H NMR is the best technique for determining T_{IN} by the real-time observation of the spectrum. Real-time ^{14}N NMR experiments were not possible because of the much lower sensitivity of this nucleus. T_{IN} was identified for high w ($> 0{\cdot}3$) samples from the first appearance of the nematic doublet on cooling from the isotropic phase. For the samples where fast chemical exchange was present, T_{IN} was indicated by an initial sudden and rapid broadening of the isotropic signal before it eventually resolved into a fast exchange doublet (see figure 4 (*b*)).

3.3. *Location of Tp (I, N, L)*

This was determined using ^2H NMR from real-time observation of the signal on cooling a $w = 0{\cdot}421$ sample from the isotropic solution phase along the isopleth shown in figure 5. On cooling below T_{IL}, the lamellar phase ($\phi = 0°$) spectrum appears (see figure 5 (*b*)) together with small $\phi = 90°$ lamellar-phase singularities which persist on cooling into the pure *L* phase. On cooling below *T*p(I, N, L), a nematic phase spectrum appears (see figure 5 (*c*)), the intensity of which grows as that of the isotropic phase signal decreases. After about 10 min at this temperature, the isotropic singlet disappears and only nematic and lamellar phases are present. On further cooling, the intensity of the nematic signal decreases in line with the lever rule, until just below T_{LI}, only the L phase spectrum is seen (see figure 5 (*d*)). The temperature at which the nematic phase signal first appeared was taken as the temperature at *T*p(I, N, L) and the compositions of the isotropic, nematic, and lamellar phases were obtained from the abscissae of the respective curves at the triple point temperature [1, 4].

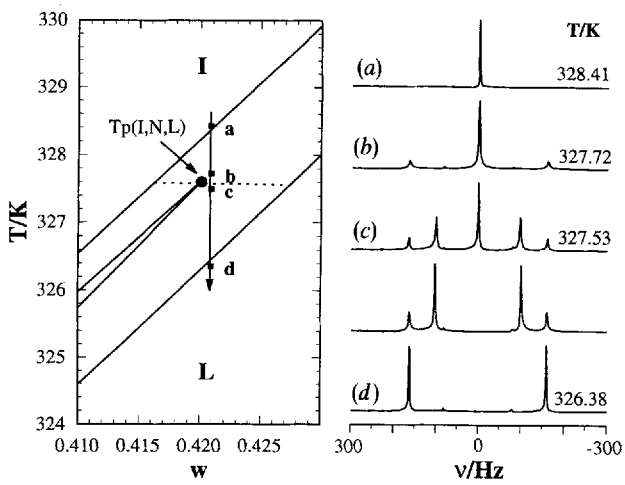

Figure 5. ^2H NMR spectra of D_2O on cooling along the isopleth shown on the partial phase diagram on the left. The nematic doublet (*c*) was first detected at 327·60 K which is taken to be the temperature of *T*p(I, N, L). The lower (*c*) spectrum was taken 10 min after the upper one. Note the appearance of the L phase doublet with $\phi = 90°$ (see legend to figure 2).

3.4. *Location of Tcp*

This was estimated as the point at which $T_{NL} - T_{LN}$, as measured by ^{14}N NMR, became zero. The advantage of ^{14}N over ^2H measurements is demonstrated in figure 6. Here $T_{NL} - T_{LN}$ is 0·42(3) K and the ^{14}N quadrupole splittings at T_{LN} and T_{NL} are, respectively, 4·60 and 3·89 kHz. The corresponding ^2H quadrupole splittings are only 220 and 186 Hz. It is clear that the ^2H quadrupole splittings in the nematic/lamellar mixed phase region are weighted averages of the nematic and lamellar values due to fast exchange of D_2O molecules between the two phases, whilst the exchange of TMA^+ ions between the two phases is slow on the NMR time-scale. On first cooling from the N_D^+ into the N_D^+/L biphasic region, the L phase is dispersed as small droplets in the N_D^+ continuous phase and the D_2O molecules and TMA^+ ions will diffuse between the two phases. Slow exchange requires $1/\tau < 2\pi\Delta$, where $\Delta = (\Delta\tilde{\nu}_L - \Delta\tilde{\nu}_N)/2$ [1]. For slow exchange, τ needs to be > 9 ms for D_2O molecules and $> 0{\cdot}5$ ms for TMA^+ ions. Assuming a diffusion coefficient of $\approx 10^{-9}\,m^2\,s^{-1}$ for both species, a D_2O molecule would diffuse a root mean square distance of 7 μm compared with only 1·7 μm for a TMA^+ ion. Thus the mean droplet diameter for slow exchange in the ^{14}N spectrum need only be about 3 μm, compared to about 14 μm in the ^2H spectrum.

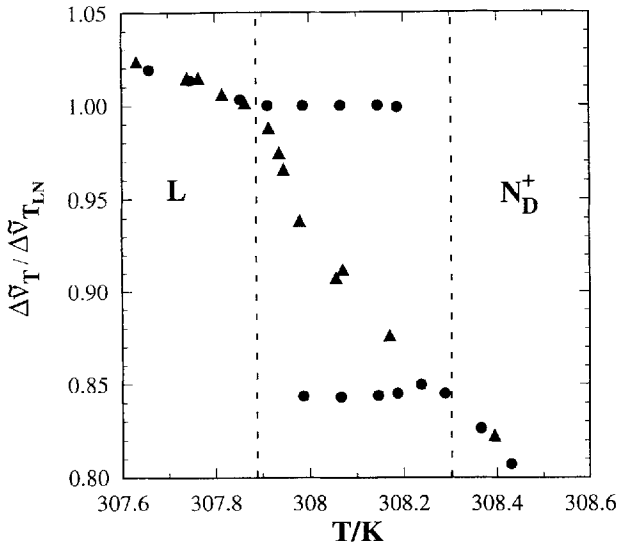

Figure 6. Temperature dependence of the partially averaged ^{14}N (●) and ^{2}H (▲) quadrupole splittings, $\Delta\bar{\nu}_T$, for the TMAHFN/D_2O ($w = 0.312$) sample, normalized to their values at T_{LN}, $\Delta\bar{\nu}_{T_{LN}}$, illustrating the superiority of ^{14}N NMR for detecting the temperature range T_{NL}–T_{LN} of the N_D^+/L biphasic region. The D_2O molecules are undergoing fast exchange between nematic and lamellar environments and the ^{2}H quadrupole splittings are the weighted mean of $\Delta\bar{\nu}(T_{LN})$ and $\Delta\bar{\nu}(T_{NL})$. The magnitudes of the ^{14}N and ^{2}H quadrupole splittings at T_{LN}, are 4·60 and 0·22 kHz, respectively.

For a $w = 0.230$ sample the ^{14}N quadrupole splittings at T_{NL} and T_{LN} are, respectively, 4·57 and 4·15 kHz and $T_{NL} - T_{LN}$ is 0·20 K. At $w = 0.184$, the ^{14}N quadrupole splittings at T_{NL} is 4·72 and no mixed phase region was detectable. *T*cp was thus estimated to be at $w = 0.20(2)$ and $T = 286(5)$ K. As for the *T*cp points along the N_D^+–L transition lines in the CsPFO [3] and APFO/D_2O [2] systems, the precise location of *T*cp in the TMAHFN/D_2O system is limited by the sensitivity of the method used to locate the point at which the N_D^+–L transition appears to become second order. It is quite possible that the N_D^+–L transition is always first order [49], though weakly so, and that *T*cp as defined here has only empirical significance.

3.5. *Location of Tp(I, N, K) and Cep*

*T*p(I, N, K) was obtained simply from the intersection of the lower boundary to the I–N_D^+ transition curve (T_{NI}) with the solubility curve *T*c, and *C*ep from the intersection of the N_D^+–L transition curve (T_{LN}) with the solubility curve.

3.6. *Comparison of phase behaviour with other perfluorinated systems*

The phase diagram for the TMAPFO/D_2O system [50] is similar to that of the TMAHFN/D_2O system, but the transition temperatures are lower by about 40 K at equivalent volume fractions and no nematic phase is present, the I–L transition occurring through an I/L biphasic region throughout the concentration range. Lowering the transition temperatures by 40 K in figure 1 places them very close to a probable solubility curve for the TMAPFO/D_2O system. This, together with an expected decrease in T_{IN}–T_{LN} on decreasing the chain length (see later), is probably the reason why no nematic phase was seen in the TMAPFO/D_2O system. It is probably present and should, in fact, be detectable at low volume fractions and temperatures.

At corresponding ϕ values, the phase transition temperatures of the CsHFN, AHFN, and TMAHFN/D_2O systems are in the order $T_{CsHFN} > T_{AHFN} > T_{TMAHFN}$. The actual T_{NI} values at $\phi = 0.15$ for the CsHFN, AHFN, and TMAHFN/D_2O systems are, respectively, 325·5 [36], 304–308 [34, 35], and 291·0 K, whilst at $\phi = 0.30$ the corresponding values are 350·5, 338–343 and 323·5 K. In the CsPFO and APFO/D_2O systems, X-ray diffraction measurements [2, 5] have shown that, at the same volume fraction of amphiphile, the micelle axial ratios (*a*/*b*) at the isotropic–nematic transition are the same in both systems [51]. In *T* versus volume fraction space, the phase diagrams of the latter two systems are quite similar, but the transition temperatures for the Cs^+ salt are about 22 K higher. The differences in the phase transition temperatures between the two systems can thus be understood in terms of changes in the micelle self-assembly on substituting NH_4^+ for Cs^+ ions. Since the micelles are essentially the same size at the transition temperatures and the micelle sizes decrease with increasing temperature [5], then at any given volume fraction and temperature the micelles must be smaller in the APFO/D_2O system. The T_{NI} order for the HFN^- systems indicates, therefore, that substitution of TMA^+ for NH_4^+ ions will lead to a decrease in micelle size.

The increase in the phase transition temperatures with increasing chain length can also be accounted for in terms of micelle self-assembly, since it has been shown that in micellar liquid crystal systems formed from the Cs^+ salts of perfluorocarboxylic acids with chain lengths from C_7 to C_{10}, both the nematic–isotropic and the lamellar–nematic transitions occur when the micelles attain a certain *a*/*b* ratio corresponding to a particular ϕ value [36]. Longer chains produce bigger micelles and, since the micelle sizes are essentially the same at the transition temperature, these increase with increasing chain length.

A detailed comparison of the phase behaviour between micellar liquid crystal systems is limited to comparisons between the present one and the only two other systems for which high resolution phase diagrams are currently available, i.e the CsPFO/water [1, 4] and APFO/D_2O [2] systems. The phase diagram of the TMAHFN/D_2O system is topologically similar to those of the CsPFO/D_2O and APFO/D_2O systems, but the volume fraction at *T*p(I, N, L)

and *T*cp are significantly lower in the TMAHFN/D_2O system ($\phi_N = 0{\cdot}325$ and $0{\cdot}14$, respectively, compared with values of $0{\cdot}455$ and $0{\cdot}36$ in the APFO/D_2O and $0{\cdot}426$ and $0{\cdot}25$ in the CsPFO/D_2O system). The volume fraction ϕ_N at *T*p(I, N, L) in the TMAHFN/D_2O system is slightly smaller than the value calculated ($\phi_N = 0{\cdot}36$) using the Taylor/Herzfeld model [40], whilst for both the CsPFO and APFO/D_2O systems the measured values are higher than the calculated value. It is not the increase in the chain lengths which is responsible for the displacement to lower volume fraction of the fixed points in the TMAHFN/D_2O system, since in aqueous solutions of discotic micelles of the caesium salts of perfluorocarboxylic acids (C_7 to C_{10} inclusive) the volume fractions at both *T*p(I, N, L) and *T*cp are practically the same irrespective of the length of the perfluorocarbon chain [36]. The other significant change brought about by substitution of TMA^+ ion for either Cs^+ or NH_4^+ ions is a large decrease in the width of the nematic phase, as measured by the quantity T_{IN}–T_{LN}. In the CsPFO/D_2O system, T_{IN}–T_{LN} is about 6 K, depending on the amphiphile composition. The corresponding value in the APFO/D_2O system is about 7 K. In the TMAHFN/D_2O system, T_{IN}–T_{LN} is only $1{\cdot}9$ K at $w = 0{\cdot}42$, increasing to $3{\cdot}9$ K at $w = 0{\cdot}15$. Again, it is not the increase in the chain length that is responsible for the decrease in T_{IN}–T_{LN}, since in Cs^+ systems, substituting HFN^- for PFO^- ions results in an increase of about 1K in T_{IN}–T_{LN} [36].

In conclusion, we have shown that the high resolution phase diagram of the TMAHFN/D_2O system has the generic form of other systems composed of solutions of discotic micelles. Differences in the phase transition temperatures in the various systems can be accounted for in terms of changes in the micelle self-assembly on changing either the counterion or the surfactant chain length. There are, however, interesting differences between the precise locations of the *T*p(I, N, L) triple point and the nematic/lamellar tricritical point *T*cp in the three systems for which high resolution phase diagrams currently exist. Substitution of TMA^+ ions for either Cs^+ or NH_4^+ ions leads to a displacement of these points to lower volume fractions.

We wish to thank Massey University for the award of a Post Doctoral Fellowship to P.J.B.E.

References

[1] Boden, N., Corne, S. A., and Jolley, K. W., 1987, *J. phys. Chem.*, **91,** 4092.
[2] Boden, N., Clements, J., Jolley, K. W., Parker, D., and Smith, M. H., 1990, *J. chem. Phys.*, **93,** 9096.
[3] Boden, N., Jolley, K. W., and Smith, M. H., 1989, *Liq. Crystals*, **6,** 481.
[4] Boden, N., Jolley, K. W., and Smith, M. H., 1993, *J. phys. Chem.*, **97,** 7678.
[5] Holmes, M. C., Reynolds, D. J., and Boden, N., 1987, *J. phys. Chem.*, **91,** 5257.
[6] Boden, N., Corne, S. A., Holmes, M. C., Jackson, P. H., Parker, D., and Jolley, K. W., 1986, *J. Phys., Paris*, **47,** 2135.
[7] Leaver, M. S., and Holmes, M. C., 1993, *J. Phys. II, Paris*, **3,** 105.
[8] Holmes, M. C., Scotta, P., Hendrikx, Y., and Deloche, B., 1993, *J. Phys. II, Paris*, **3,** 1735.
[9] Boden, N., and Jolley, K. W., 1992, *Phys. Rev.* A, **45,** 8751.
[10] Boden, N., and Holmes, M. C., 1984, *Chem. Phys. Lett.*, **109,** 76.
[11] Boden, N., Jackson, P. H., McMullen, K., and Holmes, M. C., 1979, *Chem. Phys. Lett.*, **65,** 476.
[12] Boden, N., McMullen, K., and Holmes, M. C., 1980, *Magnetic Resonance in Colloid and Interface Science*, Edited by J. P. Fraissard and H. A. Resing (Reidel), p. 667.
[13] Boden, N., Corne, S. A., and Jolley, K. W., 1984, *Chem. Phys. Lett.*, **105,** 99.
[14] Boden, N., Clements, J., Dawson, K. A., Jolley, K. W., and Parker, D., 1991, *Phys. Rev. Lett.*, **66,** 2883.
[15] Boden, N., Hedwig, G. R., Holmes, M. C., Jolley, K. W., and Parker, D., 1992, *Liq. Crystals*, **11,** 311.
[16] Jolley, K. W., Smith, M. H., and Boden, N., 1989, *Chem. Phys. Lett.*, **162,** 152.
[17] Photinos, P., and Saupe, A., 1990, *Phys. Rev.* A, **41,** 954.
[18] Photinos, P., and Saupe, A., 1991, *Phys. Rev.* A, **43,** 2890.
[19] Chung, J., and Prestegard, J. H., 1993, *J. phys. Chem.*, **97,** 9837.
[20] Rosenblatt, C., and Zolty, N., 1985, *J. Phys. Lett., Paris*, **46,** L-1191.
[21] Rosenblatt, C., 1985, *Phys. Rev.* A, **32,** 1115.
[22] Rosenblatt, C., 1985, *J. chem. Phys.*, **82,** 2790.
[23] Rosenblatt, C., Kumar, S., and Litster, J. D., 1984, *Phys. Rev.* A, **29,** 1010.
[24] Rosenblatt, C., 1987, *J. phys. Chem.*, **91,** 3830.
[25] Rosenblatt, C., 1988, *J. phys. Chem.*, **92,** 5770.
[26] Li, Z., and Rosenblatt, C., 1988, *J. chem. Phys.*, **89,** 5033.
[27] Rosenblatt, C., 1989, *J. Coll. Inter. Sci.*, **131,** 236.
[28] Shin, S. T., and Kumar, S., 1991, *Phys. Rev. Lett.*, **66,** 1062.
[29] Shin, S. T., Kumar, S., Finotello, D., Sabol Keast, S., and Neubert, M. E., 1992, *Phys. Rev.* A, **45,** 8683.
[30] Fisch, M. R., Kumar, S., and Litster, J. D., 1986, *Phys. Rev. Lett.*, **57,** 2830.
[31] Larson, B. D., and Litster, J. D., 1984, *Molec. Crystals liq. Crystals*, **113,** 13.
[32] Photinos, P., and Saupe, A., 1989, *J. chem. Phys.*, **90,** 5011.
[33] Everiss, E., Tiddy, G. J. T., and Wheeler, B. A., 1976, *J. chem. Soc. Faraday Trans. I*, **72,** 1747.
[34] Fontell, K., and Lindman, B., 1983, *J. phys. Chem.*, **87,** 3289.
[35] Reizlein, K., and Hoffmann, H., 1984, *Progr. Coll. Polym. Sci.*, **69,** 83.
[36] Parbhu, A. N., 1994, Ph.D. thesis, Massey University, New Zealand.
[37] Israelachvili, J., 1991, *Intermolecular and Surface Forces* (Academic Press), Chap. 16.
[38] McMullen, W. E., Ben-Shaul, A., and Gelbart, W. M., 1984, *J. Coll. Inter. Sci.*, **98,** 523.
[39] McMullen, W. E., Gelbart, W. M., and Ben-Shaul, A., 1984, *J. phys. Chem.*, **88,** 6649.
[40] Taylor, M. P., and Herzfeld, J., 1991, *Phys. Rev.* A, **43,** 1892.

[41] SLUCKIN, T. J., 1989, *Liq. Crystals*, **6,** 111.
[42] TAYLOR, M. P., and HERZFELD, J., 1993, *J. Phys.: Condens. Matter*, **5,** 2651.
[43] HERBST, L., HOFFMANN, H., KALUS, J., REIZLEIN, K., SCHMELZER, U., and IBEL, K., 1985, *Ber. Bunsenges. phys. Chem.*, **89,** 1050.
[44] BODEN, N., CORNE, S. A., HALFORD-MAW, P., FOGARTY, D., and JOLLEY, K. W., 1992, *J. magn. Reson.*, **98,** 92.
[45] KELL, G. S., 1967, *J. chem. Engng.*, **12,** 66.
[46] SMITH, M. H., 1990, Ph.D., Massey University, New Zealand.
[47] ABRAGHAM, A., 1962, *The Principle of Nuclear Magnetism* (Oxford University Press), Chap. 10.
[48] CHIDICHIMO, G., GOLEMME, A., RANIERI, G. A., TERENZI, M., and DOANE, J. W., 1986, *Molec. Crystals liq. Crystals*, **132,** 275.
[49] ANISIMOV, M. A., CLADIS, P. E., GORODETSKII, E. E., HUSE, D. A., TARATUTA, V. G., VAN SAARLOOS, W., and VORONOV, V. P., 1990, *Phys. Rev.* A, **41,** 6749.
[50] JACKSON, P. H., 1980, Ph.D. Leeds, England.
[51] BODEN, N., EDWARDS, P. J. B., and JOLLET, K. W., 1992, *Structure and Dynamics in Supramolecular Aggregates and Strongly Interacting Colloids*, edited by S. H. Chen, J. S. Huang and P. Tartaglia (Kluwer), p. 433.